East Asian Journal on Applied Mathematics
doi: 10.4208/eajam.150313.020513a

Vol. **3**, No. 2, pp. 93-106
May 2013

Spherical Geometry HOC Scheme to Capture Low Pressures within a Wake

T. V. S. Sekhar* and B. Hema Sundar Raju

School of Basic Sciences, Indian Institute of Technology Bhubaneswar, Bhubaneswar-751 007, India.

Received 15 March 2013; Accepted (in revised version) 2 May 2013

Available online 31 May 2013

Abstract. The solution of the pressure Poisson equation in spherical polar coordinates using a higher order compact (HOC) scheme effectively captures low pressure values in the wake region for viscous flow past a sphere. In the absence of an exact solution, the fourth-order of accuracy of the results is illustrated. Low pressure circular contours occur in the wake region when the Reynolds number $Re = 161$, which is a lower value than previously identified in the literature, and closed pressure contours appear in two regions when $Re = 250$.

AMS subject classifications: 76D05, 35Q35, 65N06

Key words: Pressure fields, low pressure, spherical geometry, higher order compact scheme, Navier-Stokes equations.

1. Introduction

Higher order compact (HOC) schemes have been used elsewhere to describe flow quite accurately — e.g. at weather warning centres and in global ocean modelling. Simpler second-order spatially accurate schemes have also been used in many computational fluid dynamics problems, but they may fail or require smaller than acceptable grid step sizes to capture the flow phenomena when the domain is large. The pressure in the entire computational domain is often important in describing the flow behaviour. Calculations by Fornberg [1] and Johnson & Patel [2] for steady viscous flow past a sphere in the entire computational domain are at most second order accurate. Recently, Sekhar *et al.* [3] developed a higher order compact scheme to solve the Navier-Stokes equations in spherical polar co-ordinates for viscous flow past a sphere. This article extends that scheme to solve the corresponding pressure Poisson equation in spherical polar coordinates, and the low pressure behaviour predicted within the wake region differs from some of the earlier results in Refs. [1, 2] and references therein.

*Corresponding author. *Email addresses:* sekhartvs@iitbbs.ac.in (T. V. S. Sekhar), srb11@iitbbs.ac.in (B. Hema Sundar Raju)

2. Basic Equations

We consider steady axisymmetric viscous incompressible flow past a sphere placed in a uniform stream with velocity U_∞ from left to right. The governing continuity and momentum equations are

$$\nabla\cdot\boldsymbol{v}=0\,, \tag{2.1}$$

$$\boldsymbol{v}\cdot\nabla\boldsymbol{v}=-\nabla p+\frac{2}{Re}\nabla^2\boldsymbol{v}\,, \tag{2.2}$$

where the relevant length scale is the radius of the sphere a but we have chosen to refer to the diameter of the sphere (and the kinematic viscosity coefficient ν) in defining the Reynolds number

$$Re=\frac{2\,U_\infty\,a}{\nu}\,.$$

The dimensionless radius of the sphere is thus $r=1$, while the dimensionless velocity $\boldsymbol{v}$ corresponds to dividing the dimensional velocity by the uniform stream velocity U_∞. In terms of a stream function ψ, in spherical polar coordinates the respective dimensionless radial and transverse velocity components are

$$v_r=\frac{1}{r^2\sin\theta}\frac{\partial\psi}{\partial\theta}\,,\qquad v_\theta=-\frac{1}{r\sin\theta}\frac{\partial\psi}{\partial r}\,, \tag{2.3}$$

such that the continuity equation (2.1) is immediately satisfied. From the well known vector identities

$$\boldsymbol{v}\cdot\nabla\boldsymbol{v}=\nabla\left(\frac{1}{2}v^2\right)-\boldsymbol{v}\times(\nabla\times\boldsymbol{v})$$

and

$$\nabla\times\nabla\times\boldsymbol{v}=\nabla(\nabla\cdot\boldsymbol{v})-\nabla^2\boldsymbol{v}\,,$$

the momentum equation (2.2) may be rewritten

$$\nabla\left(\frac{1}{2}v^2\right)-\boldsymbol{v}\times\boldsymbol{\omega}=-\nabla p-\frac{2}{Re}\nabla\times\boldsymbol{\omega} \tag{2.4}$$

where $\boldsymbol{\omega}=\nabla\times\boldsymbol{v}$ is the vorticity, and then taking the curl we obtain

$$\nabla\times(\boldsymbol{v}\times\boldsymbol{\omega})=\frac{2}{Re}\,\nabla\times\nabla\times\boldsymbol{\omega}\,. \tag{2.5}$$

2.1. The velocity field equations

Expanding Eq. (2.5) using Eq. (2.3) and applying the transformation $r=e^{\xi}$ yields the Navier-Stokes equations in terms of the dimensionless stream function and vorticity —

i.e. for axisymmetric flow (where $\partial/\partial\phi = 0$) in spherical polar coordinates (r, θ, ϕ) we obtain

$$\frac{\partial^2\psi}{\partial\xi^2} - \frac{\partial\psi}{\partial\xi} + \frac{\partial^2\psi}{\partial\theta^2} - \cot\theta\,\frac{\partial\psi}{\partial\theta} = -\sin\theta\, e^{3\xi}\,\omega \tag{2.6}$$

$$\frac{\partial^2\omega}{\partial\xi^2} + \frac{\partial\omega}{\partial\xi} + \cot\theta\,\frac{\partial\omega}{\partial\theta} + \frac{\partial^2\omega}{\partial\theta^2} - \frac{\omega}{\sin^2\theta} = \frac{Re}{2\sin\theta}\,e^{-\xi}\left(\frac{\partial\psi}{\partial\theta}\frac{\partial\omega}{\partial\xi} - \frac{\partial\psi}{\partial\xi}\frac{\partial\omega}{\partial\theta} - \frac{\partial\psi}{\partial\theta}\omega + \frac{\partial\psi}{\partial\xi}\omega\cot\theta\right), \tag{2.7}$$

where

$$v_r = \frac{e^{-2\xi}}{\sin\theta}\frac{\partial\psi}{\partial\theta}, \qquad v_\theta = -\frac{e^{-2\xi}}{\sin\theta}\frac{\partial\psi}{\partial\xi}. \tag{2.8}$$

The boundary conditions to be satisfied are:

$\psi = \dfrac{\partial\psi}{\partial\xi} = 0$, $\omega = -\dfrac{1}{\sin\theta}\dfrac{\partial^2\psi}{\partial\xi^2}$ on the surface of the sphere $(\xi = 0)$, and

$\psi \sim \dfrac{1}{2}e^{2\xi}\sin^2\theta$, $\omega \to 0$ at large distances from the sphere $(\xi \to \infty)$;

and in addition we have $\psi = 0$, $\omega = 0$ along the axis of symmetry ($\theta = 0$ and $\theta = \pi$).

The velocity field is obtained by solving Eqs. (2.6)–(2.8) using a fourth-order compact scheme, which is then used to solve the pressure Poisson equation discussed below.

2.2. The pressure Poisson equation

On taking the divergence of the momentum equation (2.2) we have

$$\nabla\cdot(\boldsymbol{v}\cdot\nabla\boldsymbol{v}) = -\nabla^2 p, \tag{2.9}$$

and on again expanding using Eq. (2.3) and applying the transformation $r = e^{\xi}$ we obtain the relevant pressure Poisson equation in spherical polar coordinates (r, θ, ϕ):

$$\begin{aligned}\frac{\partial^2 p}{\partial\xi^2} + \frac{\partial^2 p}{\partial\theta^2} + \frac{\partial p}{\partial\xi} + \cot\theta\,\frac{\partial p}{\partial\theta} \\ = -\frac{e^{-4\xi}}{\sin^2\theta}\left[\left(\frac{\partial^2\psi}{\partial\xi\partial\theta} - 2\frac{\partial\psi}{\partial\theta}\right)^2 + \left(\frac{\partial^2\psi}{\partial\xi\partial\theta} - \cot\theta\,\frac{\partial\psi}{\partial\xi}\right)^2 + 2\left(\frac{\partial\psi}{\partial\theta} - \frac{\partial^2\psi}{\partial\xi\partial\theta}\right)\frac{\partial\psi}{\partial\theta}\right. \\ \left. + \left((3+\csc^2\theta)\frac{\partial\psi}{\partial\xi} - 2\frac{\partial^2\psi}{\partial\xi^2}\right)\frac{\partial\psi}{\partial\xi} - 2\left(\frac{\partial^2\psi}{\partial\theta^2} - \cot\theta\,\frac{\partial\psi}{\partial\theta}\right)\left(\frac{\partial^2\psi}{\partial\xi^2} - 2\frac{\partial\psi}{\partial\xi}\right)\right].\end{aligned} \tag{2.10}$$

In addition, from Eq. (2.2) rewritten as

$$\nabla p = -\frac{2}{Re}\nabla\times\boldsymbol{\omega} - \boldsymbol{v}\cdot\nabla\boldsymbol{v}, \tag{2.11}$$

on once again expanding using Eq. (2.3) and applying the transformation $r = e^{\xi}$ we obtain the corresponding radial pressure component equation:

$$\frac{\partial p}{\partial \xi} = -\frac{e^{-4\xi}}{\sin^2\theta}\left[\left(\frac{\partial^2\psi}{\partial\xi\partial\theta} - 2\frac{\partial\psi}{\partial\theta}\right)\frac{\partial\psi}{\partial\theta} - \left(\frac{\partial^2\psi}{\partial\theta^2} - \cot\theta\,\frac{\partial\psi}{\partial\theta}\right)\frac{\partial\psi}{\partial\xi} - \left(\frac{\partial\psi}{\partial\xi}\right)^2\right] - \frac{2}{Re}\left(\frac{\partial\omega}{\partial\theta} + \omega\cot\theta\right). \tag{2.12}$$

On the surface of the sphere, Eq. (2.12) reduces to

$$\frac{\partial p}{\partial \xi} = -\frac{2}{Re}\left(\frac{\partial\omega}{\partial\theta} + \omega\cot\theta\right),$$

and consequently the boundary conditions to be satisfied in solving Eq. (2.10) are:

$\frac{\partial p}{\partial \xi} = -\frac{2}{Re}\left(\frac{\partial\omega}{\partial\theta} + \omega\cot\theta\right)$ on the surface of the sphere $(\xi = 0)$,

and $p \to 0$ at large distances from the sphere $(\xi \to \infty)$;

and in addition we have $\frac{\partial p}{\partial\theta} = 0$ along the axis of symmetry ($\theta = 0$ and $\theta = \pi$).

3. HOC Scheme (Fourth-Order)

The standard fourth-order central difference representation of the partial derivatives required are

$$\frac{\partial\phi}{\partial\xi} = \delta_\xi\phi - \frac{h^2}{6}\frac{\partial^3\phi}{\partial\xi^3} + \mathrm{O}(h^4), \tag{3.1}$$

$$\frac{\partial^2\phi}{\partial\xi^2} = \delta_\xi^2\phi - \frac{h^2}{12}\frac{\partial^4\phi}{\partial\xi^4} + \mathrm{O}(h^4), \tag{3.2}$$

$$\frac{\partial\phi}{\partial\theta} = \delta_\theta\phi - \frac{k^2}{6}\frac{\partial^3\phi}{\partial\theta^3} + \mathrm{O}(k^4), \tag{3.3}$$

$$\frac{\partial^2\phi}{\partial\theta^2} = \delta_\theta^2\phi - \frac{k^2}{12}\frac{\partial^4\phi}{\partial\theta^4} + \mathrm{O}(k^4), \tag{3.4}$$

where $\delta_\xi\phi$, $\delta_\xi^2\phi$, $\delta_\theta\phi$ and $\delta_\theta^2\phi$ are the standard second-order central discretisations — viz.

$$\delta_\xi\phi_{i,j} = \frac{\phi_{i+1,j} - \phi_{i-1,j}}{2h},$$

$$\delta_\xi^2\phi_{i,j} = \frac{\phi_{i+1,j} - 2\phi_{i,j} + \phi_{i-1,j}}{h^2},$$

$$\delta_\theta\phi_{i,j} = \frac{\phi_{i,j+1} - \phi_{i,j-1}}{2k},$$

$$\delta_\theta^2\phi_{i,j} = \frac{\phi_{i,j+1} - 2\phi_{i,j} + \phi_{i,j-1}}{k^2},$$

in which h and k are the grid spacings ($h \neq k$) in the radial and angular directions represented by ξ and θ, respectively. The discretisation of Eqs. (2.6) and (2.7) for the flow was detailed in Ref. [3], and the corresponding discretisation of the pressure Poisson equation (2.10) is presented below.

3.1. Discretisation of the pressure Poisson equation

Eq. (2.10) can be rewritten as

$$\frac{\partial^2 p}{\partial \xi^2} + \frac{\partial^2 p}{\partial \theta^2} + \frac{\partial p}{\partial \xi} + \cot\theta \, \frac{\partial p}{\partial \theta} = \tau_{i,j} \,, \tag{3.5}$$

where

$$\tau_{i,j} = \left[-\frac{e^{-4\xi}}{\sin^2\theta} \left\{ \left(\frac{\partial^2 \psi}{\partial \xi \partial \theta} - 2\frac{\partial \psi}{\partial \theta} \right)^2 + \left(\frac{\partial^2 \psi}{\partial \xi \partial \theta} - \cot\theta \, \frac{\partial \psi}{\partial \xi} \right)^2 + 2\left(\frac{\partial \psi}{\partial \theta} - \frac{\partial^2 \psi}{\partial \xi \partial \theta} \right) \frac{\partial \psi}{\partial \theta} \right.$$
$$\left. + \left((3 + \csc^2\theta) \frac{\partial \psi}{\partial \xi} - 2\frac{\partial^2 \psi}{\partial \xi^2} \right) \frac{\partial \psi}{\partial \xi} - 2\left(\frac{\partial^2 \psi}{\partial \theta^2} - \cot\theta \, \frac{\partial \psi}{\partial \theta} \right) \left(\frac{\partial^2 \psi}{\partial \xi^2} - 2\frac{\partial \psi}{\partial \xi} \right) \right\} \right] .$$

On introducing (3.1)-(3.4), we obtain

$$\delta_\xi^2 p_{i,j} + \delta_\theta^2 p_{i,j} + \delta_\xi p_{i,j} + \cot\theta \, \delta_\theta p_{i,j} - \alpha_{i,j} = \tau_{i,j} \,, \tag{3.6}$$

where the truncation error is

$$\alpha_{i,j} = \left[\left(\frac{h^2}{12} \frac{\partial^4 p}{\partial \xi^4} + \frac{k^2}{12} \frac{\partial^4 p}{\partial \theta^4} \right) + \left(\frac{h^2}{6} \frac{\partial^3 p}{\partial \xi^3} + \frac{k^2}{6} \cot\theta \, \frac{\partial^3 p}{\partial \theta^3} \right) \right]_{i,j} + \mathrm{O}(h^4, k^4) \,. \tag{3.7}$$

Successive partial differentiations of the rewritten Poisson equation (3.5) with respect to ξ and θ yield

$$\frac{\partial^3 p}{\partial \xi^3} = -\frac{\partial^2 p}{\partial \xi^2} - \frac{\partial^3 p}{\partial \xi \partial \theta^2} - \cot\theta \, \frac{\partial^2 p}{\partial \xi \partial \theta} + \frac{\partial \tau}{\partial \xi} \,, \tag{3.8}$$

$$\frac{\partial^4 p}{\partial \xi^4} = -\frac{\partial^4 p}{\partial \xi^2 \partial \theta^2} + \frac{\partial^3 p}{\partial \xi \partial \theta^2} - \cot\theta \, \frac{\partial^3 p}{\partial \xi^2 \partial \theta} + \cot\theta \, \frac{\partial^2 p}{\partial \xi \partial \theta} + \frac{\partial^2 p}{\partial \xi^2} + \frac{\partial^2 \tau}{\partial \xi^2} - \frac{\partial \tau}{\partial \xi} \,, \tag{3.9}$$

$$\frac{\partial^3 p}{\partial \theta^3} = -\frac{\partial^3 p}{\partial \xi^2 \partial \theta} - \frac{\partial^2 p}{\partial \xi \partial \theta} - \cot\theta \, \frac{\partial^2 p}{\partial \theta^2} + \csc^2\theta \, \frac{\partial p}{\partial \theta} + \frac{\partial \tau}{\partial \theta} \,, \text{ and} \tag{3.10}$$

$$\frac{\partial^4 p}{\partial \theta^4} = -\frac{\partial^4 p}{\partial \xi^2 \partial \theta^2} - \frac{\partial^3 p}{\partial \xi \partial \theta^2} + \cot\theta \, \frac{\partial^3 p}{\partial \xi^2 \partial \theta} + \cot\theta \, \frac{\partial^2 p}{\partial \xi \partial \theta} + \left(\cot^2\theta + 2\csc^2\theta \right) \frac{\partial^2 p}{\partial \theta^2}$$
$$- 3\csc^2\theta \cot\theta \, \frac{\partial p}{\partial \theta} + \frac{\partial^2 \tau}{\partial \theta^2} - \cot\theta \, \frac{\partial \tau}{\partial \theta} . \tag{3.11}$$

Invoking (3.8)-(3.11) in Eq. (3.6), we finally obtain

$$\begin{aligned} & d_1\delta_\xi^2 p_{i,j} + \beta_{i,j}\delta_\theta^2 p_{i,j} + \delta_\xi p_{i,j} + \gamma_{i,j}\delta_\theta p_{i,j} \\ & \quad - \frac{h^2}{12}\left(\delta_\xi^2\tau_{i,j} + \delta_\xi\tau_{i,j}\right) - \frac{k^2}{12}\left(\delta_\theta^2\tau_{i,j} + \cot\theta\,\delta_\theta\tau_{i,j}\right) \\ & \quad + d_2\left(\delta_\xi^2\delta_\theta^2 p_{i,j} + \delta_\xi\delta_\theta^2 p_{i,j} + \cot\theta\,\delta_\xi^2\delta_\theta p_{i,j} + \cot\theta\,\delta_\xi\delta_\theta p_{i,j}\right) = 0\,, \end{aligned} \tag{3.12}$$

where

$$\begin{aligned} d_1 &= 1 + \frac{h^2}{12}\,, \\ d_2 &= \frac{h^2 + k^2}{12}\,, \\ \beta_{i,j} &= 1 + \frac{k^2}{12}\left(\cot^2\theta - 2\csc^2\theta\right)\,, \\ \gamma_{i,j} &= \left(1 + \frac{k^2}{12}\csc^2\theta\right)\cot\theta\,. \end{aligned}$$

Eq. (3.12) is the fourth-order approximation to the pressure Poisson equation (3.5), where the right-hand side is approximated by a fourth-order compact stencil, except for the cross-derivative term $\partial^2\psi/\partial\xi\partial\theta$ in which the usual fourth-order central differences are one-sided near the boundaries.

3.2. Discretisation of the boundary conditions

In evaluating the boundary conditions along the axis of symmetry, the derivative $\partial p/\partial\theta$ is approximated by a fourth-order forward difference along $\theta = 0$ (at $j = 1$) and a fourth-order backward difference along $\theta = \pi$ (at $j = m+1$) — i.e.

$$\begin{aligned} p(i,1) &= \frac{1}{25}\left[48p(i,2) - 36p(i,3) + 16p(i.4) - 3p(i,5)\right]\,, \\ p(i,m+1) &= \frac{1}{25}\left[48p(i,m) - 36p(i,m-1) + 16p(i,m-2) - 3p(i,m-3)\right]\,. \end{aligned}$$

4. Results and Discussion

The solution for the viscous flow past a sphere in the vorticity-stream function formulation (2.6) and (2.7) was obtained using the higher order compact (HOC) scheme of Ref. [3] with a large far field of 100 times the radius of the sphere, and the fourth-order accuracy of the results has previously been illustrated [4]. The program is executable up to $Re = 500$, and the predicted steady axisymmetric flow up to $Re = 200$ is comparable to the results in Refs. [2, 5]. The flow for $Re = 250$ was also obtained, comparable with the steady axisymmetric results of Ref. [6]. The pressure in the entire computational domain

was obtained by solving the fourth-order discretised pressure Poisson equation (3.12) using Gauss-Seidel iteration, with the boundary conditions for the pressure p updated after every iteration and the iteration process continued until the norm of the dynamic residuals became less than 10^{-8}.

The surface pressure on the sphere was also calculated from the vorticity field using

$$p(\xi=0,\theta)=1+\frac{8}{Re}\int_0^{\infty}\left(\frac{\partial\omega}{\partial\theta}\right)_{\theta=\pi}d\xi+\frac{4}{Re}\int_{\pi}^{0}\left(\omega+\frac{\partial\omega}{\partial\xi}\right)_{\xi=0}d\theta\,. \tag{4.1}$$

The calculated surface pressure values at the rear stagnation point obtained from different grids for $Re=100$, 162 and 200 are tabulated in Table 1, demonstrating that there is grid independence.

In the absence of an exact solution, the rate of convergence of the pressure at the rear stagnation point (i.e. for the value $p(0,0)$) was tested by forming divided differences representing $dp(0,0)/dh$ for various Re with respect to the step size h for the data in Table 1. The decay of $dp(0,0)/dh$ as a function of h is shown in Fig. 1 on a log-log scale, where the value of "h" on the x-axis is taken to be the average of the grid step sizes corresponding to the divided differences. The slopes of the curves in Fig. 1 are consistent with the dotted line varying as $O(h^3)$, showing that $dp(0,0)/dh=O(h^3)$ — i.e. the results are fourth-order accurate.

The results obtained for different Reynolds numbers are presented in Fig. 2. The pattern of the graphs is consistent with those of Fornberg [1], Lee [6] and Dennis and Walker [7]. The pressures obtained at the front and rear stagnation points on the sphere (cf. Table 2) are consistent with the results of Chang & Maxey [8] and Dennis & Walker [7], and agree with the values obtained from Eq. (4.1). However, to test the accuracy of the pressure coefficient values within the wake region where low pressure contours exists, a point at 1.77828 times the radius of the sphere and 11.25° from the rear stagnation point was considered with four grids — viz. 112^2, 128^2, 224^2 and 256^2 as mentioned in Table 3. The decay of dp/dh as a function of h is presented in Fig. 3 on a log-log scale. The slopes of the curves in Fig. 3 for $Re=40$, 100 and 200 are almost parallel to the dotted line varying as $O(h^3)$, such that the results within the complicated wake region vary in order of accuracy from approximately 3.3 to 3.6.

Separation initially occurs around $Re=21$ and the separation point increases as Re increases as expected, since the adverse pressure gradient in the outflow region increases as Re increases — cf. Fig. 4(a). The transverse velocity gradient in the radial direction on the

Table 1: Grid independence of fourth-order accurate surface pressure values at rear stagnation point for $Re=100,162$ and 200. The value in the bracket is the step size h of the grid.

Re	98^2 (0.04699154)	112^2 (0.0411176)	128^2 (0.0359779)	152^2 (0.0302972)	196^2 (0.02349577)	224^2 (0.0205588)	256^2 (0.01798895)
100	-0.097466	-0.117502	-0.130041	-0.138999	-0.144643	-0.145876	-0.146578
162	-0.012129	-0.051629	-0.080275	-0.102979	-0.118140	-0.121383	-0.123299
200	-0.044174	-0.002763	-0.040521	-0.073070	-0.096182	-0.101623	-0.104712

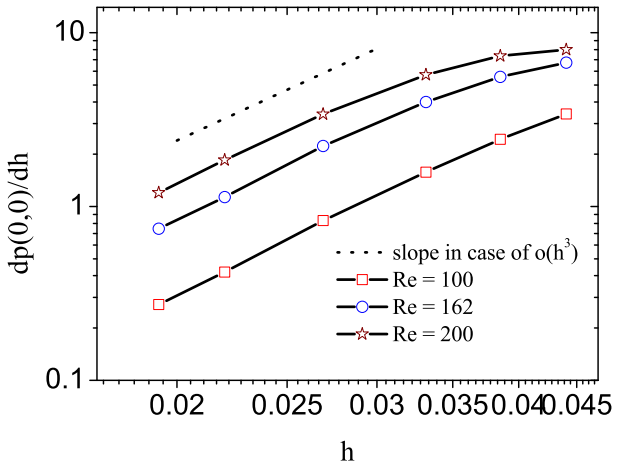

Figure 1: Decay of $dp(0,0)/dh$ as a function of h.

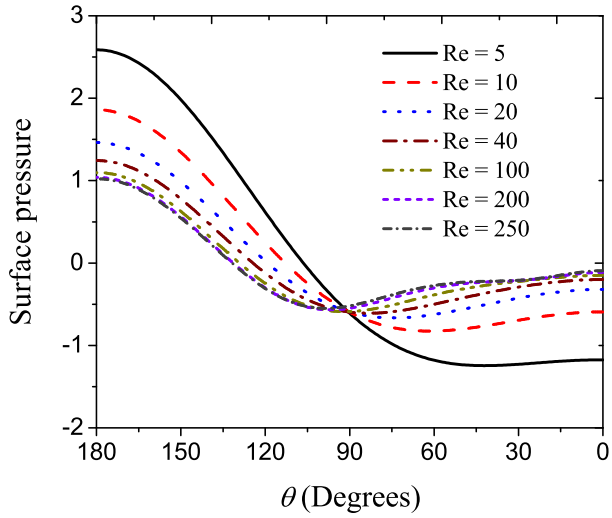

Figure 2: Angular variation of the surface pressure at the sphere for various Reynolds numbers Re.

surface of the sphere is shown in Fig. 4(b) for $0 < Re \leq 250$, where $\partial v_\theta/\partial r = 0$ indicates the point of separation. The radial velocity gradient at the surface of the sphere is shown in Fig. 4(c), where $\partial v_r/\partial r < 0$ in the wake region. The streamlines for $Re = 161, 180, 200$ and 250 are shown in Fig. 5(a)-(d), respectively. The fourth-order accurate pressure fields for $Re = 5$, 40, 100, 200 and 250 far downstream are presented in Figs. 6(a)-(e), respectively. The patterns of the pressure fields, involving positive pressure contours in the far downstream from $Re = 40$ in the present study, resemble those seen from $Re = 500$ in Ref. [1]. The pressure fields for $Re = 161$, 180, 200 and 250 near the surface of the sphere are presented in Figs. 7(a)-(d), respectively. In Fig. 7, the pressure contours are drawn in increments of 0.02 for negative values and 0.05 for positive values. Low pressure circular

Table 2: Pressures obtained at the front and rear stagnation points from Eq. (4.1), compared with previous values found in the literature.

Re	Ref. [7]		Ref. [8]	Using (4.1)		Poisson Equation	
	$p(0)$	$p(\pi)$	$p(\pi)$	$p(0)$	$p(\pi)$	$p(0)$	$p(\pi)$
5	-1.20	2.60	2.61	-1.1748	2.5853	-1.1743	2.5859
10	-0.65	1.88	1.87	-0.5928	1.8580	-0.5927	1.8583
20	-0.32	1.47	1.46	-0.3195	1.4614	-0.3194	1.4615
40	-0.19	1.26	1.25	-0.1997	1.2452	-0.1997	1.2451
100	–	–	–	-0.1466	1.1041	-0.1475	1.1030
200	–	–	–	-0.1047	1.0536	-0.1089	1.0501
250	–	–	–	-0.0772	1.0431	-0.0839	1.0384

Table 3: Pressures at the point $(1.77828, 11.25°)$ in the wake region for $Re = 40, 100$ and 200.

Re	112^2	128^2	224^2	256^2
40	-0.141503	-0.141025	-0.140335	-0.140288
100	-0.154841	-0.153324	-0.151032	-0.150888
200	-0.221701	-0.217766	-0.211746	-0.211326

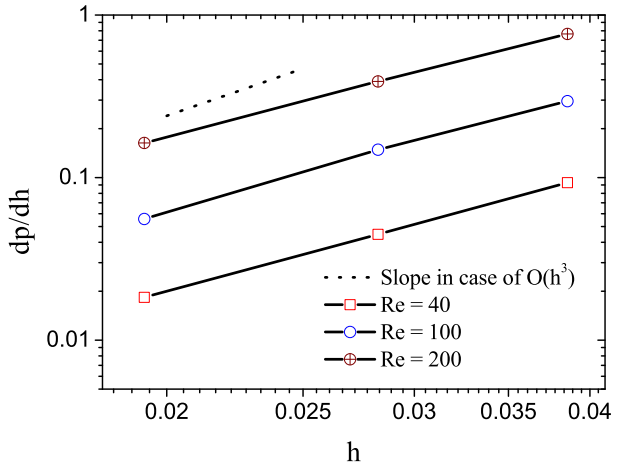

Figure 3: Decay of dp/dh as a function of h.

contours were expected within the wake region in the vicinity of the toroidal vertex, and they were found to arise at $Re = 161$ rather than at $Re = 200$ as predicted by Johnson & Patel [2] in their three-dimensional numerical simulations. This phenomenon was also observed by Fornberg [1] at $Re = 500$. In the present study, at $Re = 161$ a low pressure circle was found in the wake region with pressure minimum located at -0.21225 — cf. Fig. 7(a). At $Re = 180$, low pressure circles in the wake region ranging from -0.2126 to -0.21949 were found, with the lowest pressure located at -0.21949 — cf. Fig. 7(b).

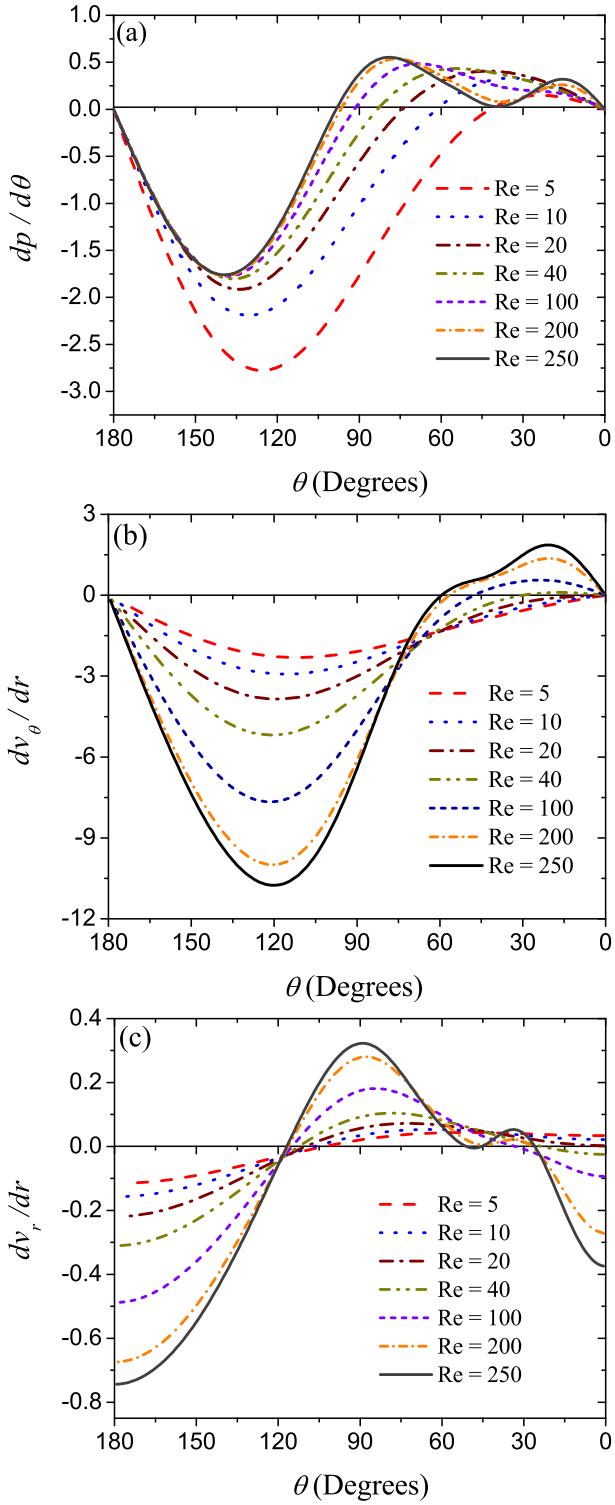

Figure 4: Angular variation of (a) pressure gradient (b) transverse velocity gradient (c) radial velocity gradient, along the surface of the sphere for different Reynolds numbers using the HOC scheme.

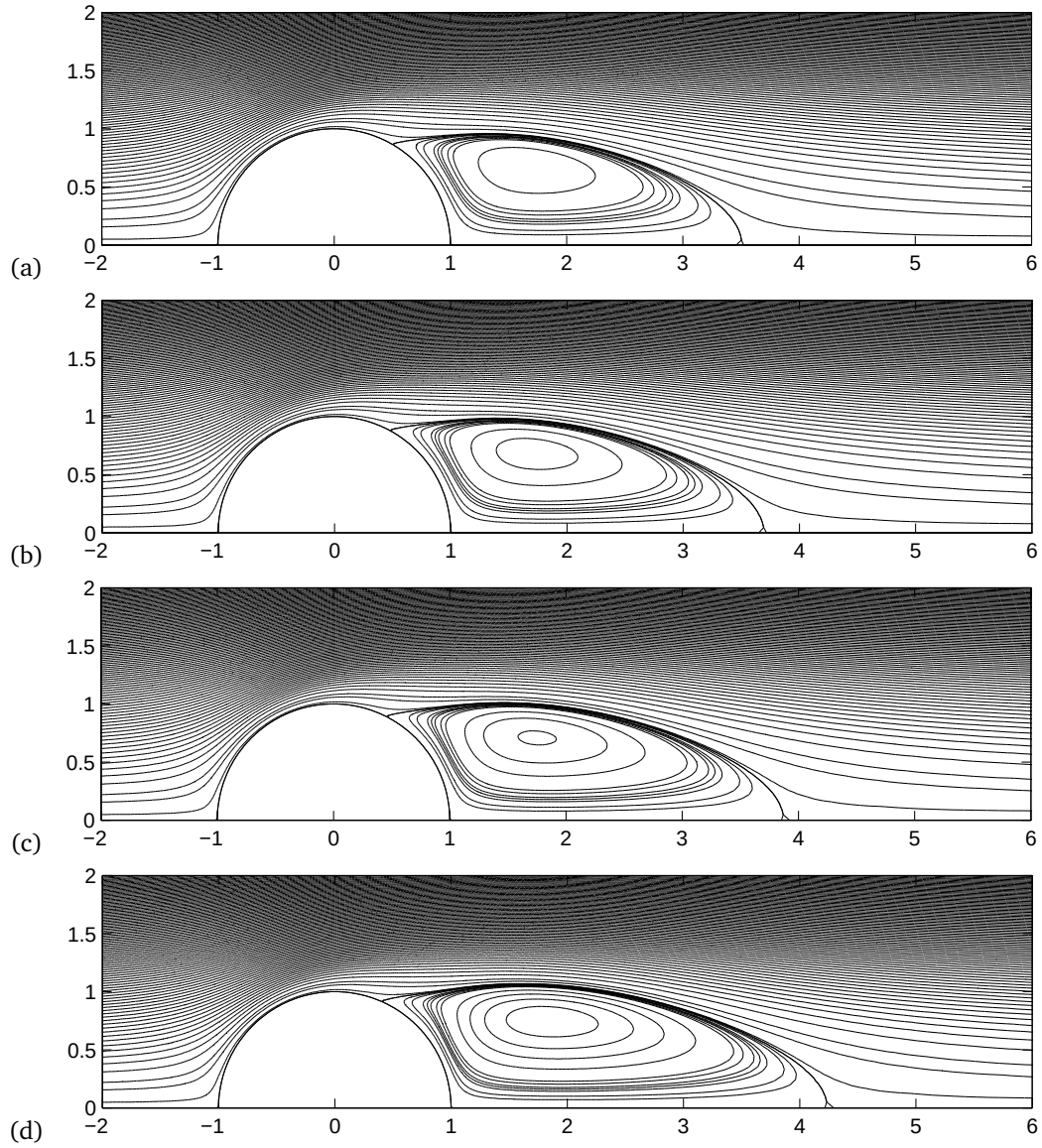

Figure 5: Streamlines using the HOC scheme for (a) $Re = 161$ (b) $Re = 180$ (c) $Re = 200$ (d) $Re = 250$. The contours are drawn for negative values in the ranges 0.01(0.01)0.08 and 0.1(0.1)0.9, and for positive values in the range 0.1(0.02)2.1.

At $Re = 200$, low pressure circles ranging from -0.211 to -0.2291 were also observed, with the lowest pressure located at -0.2291 within the wake region — cf. Fig. 7(c). At $Re = 250$, it is notable that low pressure circles were found in two regions ranging from -0.2281 to -0.25586, with the lowest pressure located at -0.25586 inside the wake as seen in Fig. 7(d), and in the other region the range is from -0.201 to -0.202 near the body surface. We note that Fornberg [1] found this type of regime at $Re \geq 1000$. The non-

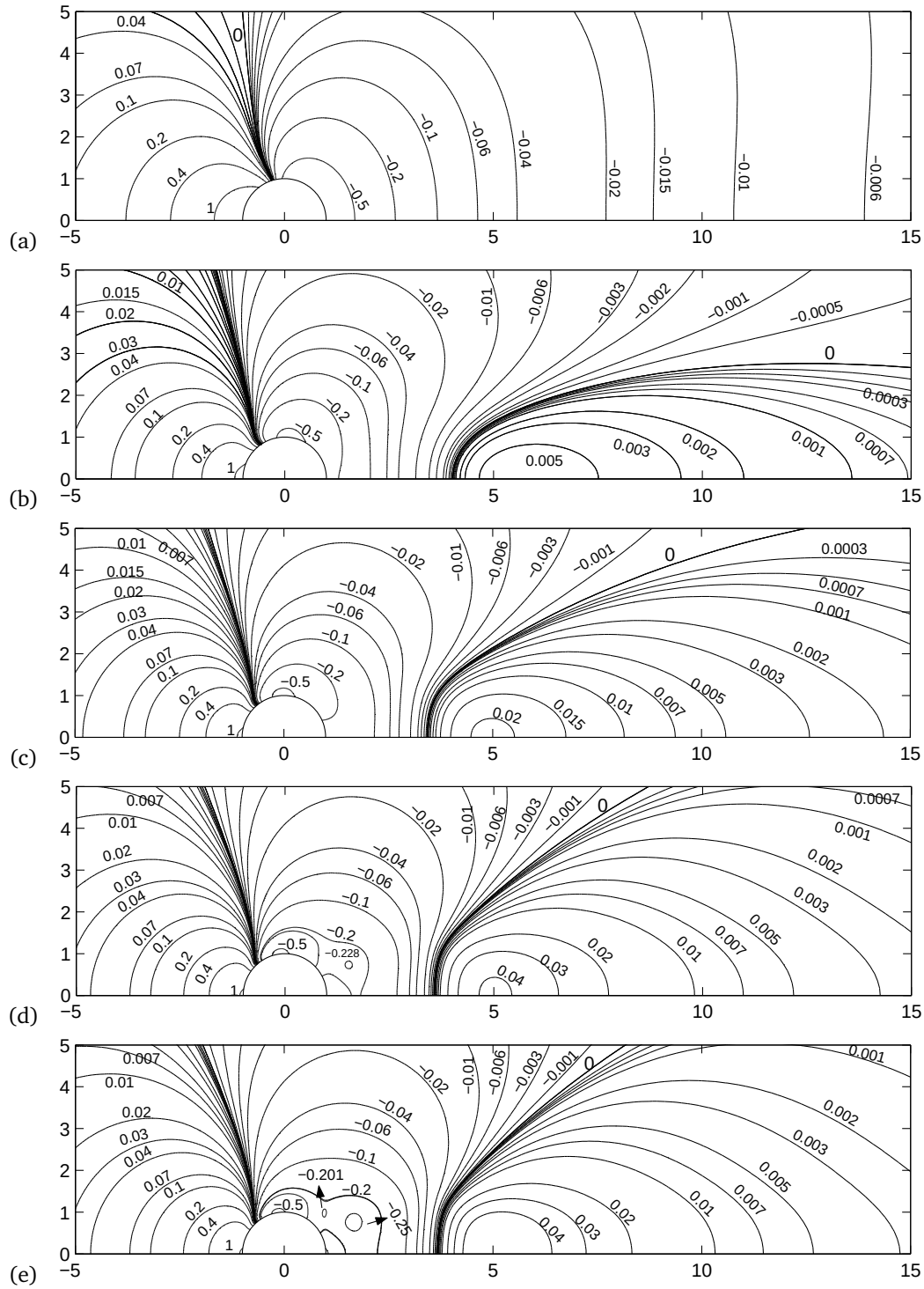

Figure 6: Pressure fields far downstream using the HOC scheme: (a) $Re = 5$ (b) $Re = 40$ (c) $Re = 100$ (d) $Re = 200$ and (e) $Re = 250$.

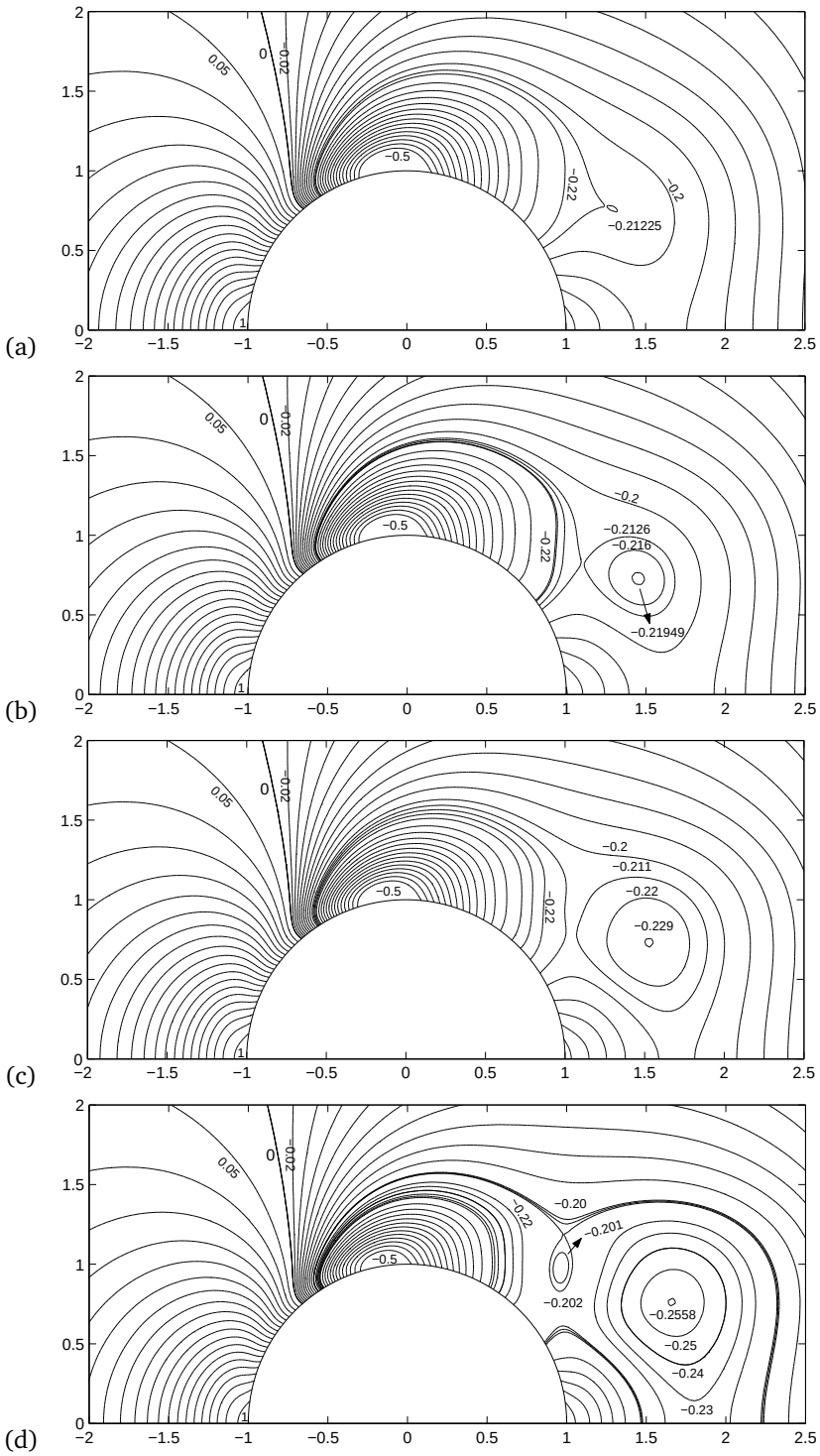

Figure 7: Pressure fields near the surface of the sphere using the HOC scheme: (a) $Re = 161$ (b) $Re = 180$ (c) $Re = 200$ (d) $Re = 250$.

existence of low pressure circles for $Re < 161$ could be due to the balance of centrifugal force of the vortex rotation by viscous forces, as mentioned by Johnson & Patel [2].

5. Conclusions

A higher order compact (HOC) scheme in spherical geometry has been developed to capture low pressures more effectively for viscous flow past a sphere. The pressure Poisson equation in spherical polar coordinates is solved by this scheme, and despite the absence of an exact solution the accuracy of the fourth-order scheme is illustrated. Although the basic flow agrees well with second-order accurate schemes, the critical values of Re where low pressure circles and pressure minima within the wake region occur differ significantly, as evidence for the superiority of the fourth-order scheme in capturing low pressures effectively (especially in large domains).

Acknowledgments

The authors thank Professor B. Fornberg (Department of Applied Mathematics, University of Colorado, USA) for his valuable suggestions.

References

[1] B. Fornberg, *Steady viscous flow past a sphere at high Reynolds numbers,* J. Fluid Mech., **190**, 471–489 (1988).

[2] T.A. Johnson and V.C. Patel, *Flow past a sphere up to a Reynolds number of 300,* J. Fluid Mech., **378**, 19–70 (1999).

[3] T.V.S. Sekhar, B. Hema Sundar Raju, and Y.V.S.S. Sanyasiraju, *Higher-order compact scheme for the incompressible Navier-Stokes equations in spherical geometry,* Comm. Comp. Phys., **11**, 99–113 (2012).

[4] T.V.S. Sekhar and B. Hema Sundar Raju, *An efficient higher-order compact scheme to capture heat transfer solutions in spherical geometry,* Comp. Phys. Comm., **183**, 2335–45 (2012).

[5] A.G. Tomboulides and S.A. Orszag, *Numerical investigation of transitional and weak turbulent flow past a sphere,* J. Fluid Mech., **416**, 45–73 (2000).

[6] S. Lee, *A numerical study of the unsteady wake behind a sphere in a uniform flow at moderate Reynolds numbers,* Computers and Fluids, **29**, 639–667 (2000).

[7] S.C.R. Dennis and J.D.A. Walker, Calculations of the steady flow past a sphere at low and moderate Reynolds numbers, J. Fluid Mech., **48**, 771–789 (1971).

[8] E.J. Chang and M.R. Maxey, Unsteady flow about a sphere at low to moderate Reynolds numbers, J. Fluid Mech., **277**, 347–379 (1994).